A High Efficiency Step-Up Current-Fed Push-Pull Quasi-Resonant Converter with Fewer Components for Fuel Cell Application

Qunfang Wu, *Student Member, IEEE*, Qin Wang, *Member, IEEE,* Jialin Xu*,* Hongxu Li and Lan Xiao, *Member, IEEE*

***Abstract*—In this paper, a new high efficiency step-up current-fed push-pull quasi-resonant converter is proposed, which is suitable for low-voltage fuel cell power conditioning system. The proposed converter conserves inherent advantages of low input-current stress and high voltage conversion ratio of the conventional current-fed push-pull converter. All of power devices can achieve soft-switching at light load improving the overall efficiency. Moreover, similar features have been obtained with fewer components in comparison with the active-clamped current-fed push-pull converter [37] and current-fed push-pull resonant converter [40], that enabling to reduce the cost and improve system reliability. In addition, the voltage-doubler rectifier is adopted to eliminate the reverse-recovery problem of secondary diodes and provides much higher voltage conversion ratio resulting in small turn-ratio of the high frequency transformer. Detailed operation, analysis, design, comparative study, experimental results and loss breakdown for the proposed converter are presented in the article. A 510 W prototype verifies the theoretical analysis and the effectiveness of the proposed concept.**

***Index Terms*—Current-fed, push-pull converter, fewer components, fuel cell, step-up**

I. INTRODUCTION

RECENTLY, the worldwide environmental pollution and energy crisis have been aggravated by the extensive exploitation of fossil fuels and the huge demand for energy. With regard to these problems, many countries are actively developing distributed power system using renewable energy sources, such as fuel cell, solar and wind energy [1]. Fuel cell has received great attention as a source of renewable energy, which is electrochemical device that converts chemical energy to electric power [2]. Usually, the output voltages of individual fuel cell stacks are below 100V dc [3] and therefore, high step-up dc/dc front-end converters with high frequency, high conversion ratio, low input current ripple and galvanic isolation are required to acquire a 350–450 V high-voltage for interfacing fuel cell stacks to the utility grid [4],[5].

Among these numerous dc/dc converters, the step-up converter suitable for fuel cell applications can be categorized as either voltage-fed [4], [6]-[10] or current-fed type [11]-[14]. An important advantage of voltage-fed type is the low switch voltage rating that enabling the use of devices with low $R_{ds(on)}$. This is greatly beneficial in the low-voltage high-current application such as fuel cells. In addition, this type does not have a self-start problem reducing the complexity of system. However, the voltage-fed step-up converters have several limitations in the fuel cells application, i.e., high transformer turns ratio which results in large leakage inductance leading to large duty cycle loss (if inductive output filter), high pulsating input current which requires an *LC* filter causing additional power loss and size, high circulating current through primary switches and the windings of transformer and severe ringing on the secondary rectifier diodes. Compared with voltage-fed type, the current-fed type has inherently a smaller input ripple and a lower HF transformer turns ratio due to the input inductor providing filtering and voltage boosting, a lower rectifier diode rating due to the negligible diode ringing and effective voltage clamping, a low risk of transformer saturation and no the problem of duty cycle [15]-[16].Therefore, the current-fed step-up converters may be meritorious over the voltage-fed converters for low-voltage high-current input applications [3].

Generally, the isolated current-fed converters have many topologies, i.e., full bridge [11]-[12], L-type half bridge [17]-[19], dual-boost [20]-[22], flyback [23]-[24], flyback-forward [25]-[26] and push-pull [27]-[41]. Each topology has its merits and dismerits. The push-pull converter is attractive owing to only two primary switches with simple circuitry, galvanic isolation, high-voltage conversion ratio and better transformer utilization. However, the conventional current-fed push-pull converter [27], [28] suffers from several drawbacks such as high voltage spikes of switches resulting from the leakage inductance of HF transformer, high voltage ratio and reverse recovery effect of the secondary rectifier diode and high power loss because of the hard-switching of devices. To resolve or mitigate these problems, usually the

Manuscript received July 01, 2016; revised September 26, 2016; accepted October 30, 2016. This work was supported by the Funding of Jiangsu Innovation Program for Graduate Education under Grant KYLX15_0275 and by the Jangsu Qing Lan Project and Jiangsu province university outstanding science and technology innovation team project.

The authors are with the Jiangsu Key Laboratory of New Energy Generation and Power Conversion, College of Automation Engineering, Nanjing University of Aeronautics and Astronautics, Nanjing 210016, China (e-mal: qfwu55@163.com; wangqin@nuaa.edu.cn; jialinxu_nuaa@163.com; 522201410@qq.com; xiaolan@nuaa.edu.cn).

This article has been accepted for publication in a future issue of this journal, but has not been fully edited. Content may change prior to final publication. Citation information: DOI 10.1109/TIE.2016.2638800, IEEE Transactions on Industrial Electronics

resonant techniques have been proposed to optimize the performance of the conventional current-fed push-pull converter. The different approaches of current-fed push-pull resonant converters are presented in [29]-[35], which utilize circuit parasitics or resonant tank to assist in zero-voltage-switching (ZVS) or zero-current-switching (ZCS) of power devices. This advantage allows reducing switching losses and achieving more efficient converters. However, in [29] and [30], the output voltage is unregulated and only determined by the input voltage and turns ratio of HF transformer. Reference in [31]-[33] can realize the output voltage regulation, but the variable frequency modulation is necessary. This aspect makes the control implementation and magnetic design complex and challenging. Moreover, a buck converter in series with the soft-switching current-fed resonant converter has been presented in [34], [35], which can achieve the voltage regulation from input to output. Obviously, the addition of buck converter produces more power loss.

It is worth noticing that one other drawback of the push-pull converter is the high turn-off voltage spike across the switch. Normally, the passive snubber [38] and active clamp circuits [9], [37]-[41], or the energy recovery snubber [42]-[43] are employed to absorb this spike. In passive snubber, such as a resistor-capacitor-diode (RCD), the energy absorbed by snubber capacitor is dissipated in the resistor causing low efficiency. The energy recovery snubber in [42] uses many devices and the method in [43] utilizes a switching converter to transfer the absorbed power back to the input voltage source. They are rather more complicated. The active snubber has more attractive since it can absorb the turn-off voltage spike, as well as assisting in soft-switching of switches. In [9], the voltage stress of primary switches can be suppressed and is less than two times of the input voltage. However, it needs two switches conduction simultaneously causing more conduction loss when the energy transfers to the load. The ZVS clamping-mode current-fed push-pull converter in [37], although can clamp a surge voltage and achieve ZVS of switches, ZVS does not enhance the efficiency sufficiently since the energy stored in the output capacitances of switches is small in low input voltage, moreover, the ZVS condition needs a larger leakage inductance or an resonant inductor resulting in additional power loss. The active soft-commutation technique is proposed in [38], which diverts the switch current each other by transformer to realize natural commutation, thereby reducing the requirement of snubber. However, it just can be achieved through the control of secondary switch and, thus, it is only suitable for the bidirectional converter. An interesting type of high step-up current resonant push-pull converter with high efficiency is presented [3], [39]-[40] for fuel cell power conditioning, which conserves inherent of a conventional current-fed push-pull converter such as low input-current stress, high voltage conversion and fixed frequency operation. In addition, a voltage-doubler rectifier is used to eliminate the reverse-recovery problem of rectifying diodes and provide higher voltage conversion. Another topology usually utilized in fuel cell applications is current-fed full bridge converter [6], [11]-[12]. Compared with the push-pull converter, the full bridge converter requires more switches and complex drive control.

With the requirements of fuel cell power conditioning system, and after reviewing different topologies, a novel simple step-up current-fed quasi-resonant converter with fewer components is proposed in this paper, as shown in Fig.1. The proposed converter consists of a current-fed push-pull structure with changing the position of two main switches, an active-clamp circuit and a voltage-doubler rectifier. ZVS can be realized for all of three primary switches at light load and ZCS of the secondary diodes can be achieved in the full load range. These aspects make this converter enable high conversion efficiency for the low input-voltage high-power fuel cell application. Moreover, compared with the similar topologies, this converter realizes the similar features with fewer components reducing the cost and improving system reliability.

This paper is organized as follows. Section II shows the topology structure and the steady-state operation of the proposed converter. In Section III, the characteristics and design procedure are analyzed deeply and followed by the topology comparative study in Section IV. Subsequently, the experimental results are provided in Section V. Section VI gives the conclusion of this paper.

II. Operation of the Proposed Converter

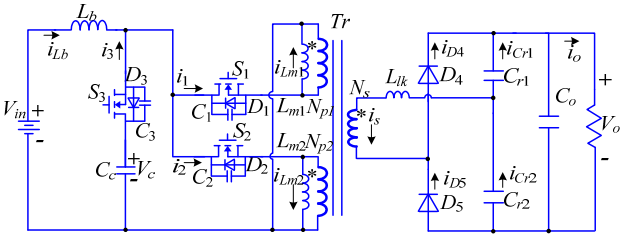

Fig. 1. Proposed current-fed push-pull quasi-resonant converter

Fig. 1 shows the schematic of the proposed current-fed push-pull quasi-resonant converter. The main components in Fig.1 are: two main switches S_1 and S_2, one auxiliary switch S_3 and a clamping capacitor C_c, an input voltage source V_{in} and an input inductor L_b are located at the primary side. A high frequency (HF) transformer Tr is represented by the primary windings N_{p1} and N_{p2} and the secondary windings N_s. The leakage inductance of Tr is referred to the secondary side by L_{lk}. In addition, the output is constituted by a voltage-doubler rectifer circuit that composing of diodes D_4, D_5 and capacitors C_{r1}, C_{r2} and C_o. Moreover, diodes D_1~D_3 are the antiparallel body diodes of the switches S_1~S_3, respectively.

Some assumptions are made to simplify the description:

1) All switches S_1~S_3 are ideal devices with antiparallel body diodes D_1~D_3 and body capacitors C_1~C_3. Diodes D_4~D_5 are ideal diodes.

2) Capacitors C_c and C_o are large enough, the voltage across them can be considered as two constants.

3) C_{r1} is equal to C_{r2} to realize symmertric working, C_{r1}=C_{r2}=C_r and C_1=C_2=C_3.

This article has been accepted for publication in a future issue of this journal, but has not been fully edited. Content may change prior to final publication. Citation information: DOI 10.1109/TIE.2016.2638800, IEEE Transactions on Industrial Electronics

4) The transformer turns ratio is N_s:N_{p1}=N_s:N_{p2}=n and the magnetizing inductance is L_{m1}=L_{m2}=L_m, the leakage inductance is smaller than the magnetizing inductance.

5) The input inductor L_b is sufficiently large so that the input current through it is constant during the switching period.

The output voltage can be controlled by PWM with a constant switching frequency. The gating signals are two 180° out-of-phase pulses of equal width with a duty cycle D greater than 50% to drive the main switches S_1 and S_2, and a complementary pulse with S_1 and S_2 to drive the auxiliary switch S_3. It is noted that the duty cycle of main switches S_1 and S_2 is always kept greater than 50% to prevent increased circulating current through the auxiliary active-clamp circuit. Operation of the converter with duty cycle less than 50% results in unwanted conduction power loss and low efficiency [12]. Fig.2 shows the key waveforms of the proposed converter operating at the steady-state, where T_s is the switching period of main switches. The overlapping region varies with duty cycle, which varies with the input voltage changing. Each switching period in the steady-state operation can be divided into ten stages. Due to the symmetry of the topology, only the former five stages are analyzed at length here and the corresponding equivalent circuits for each stage are illustrated in Fig.3.

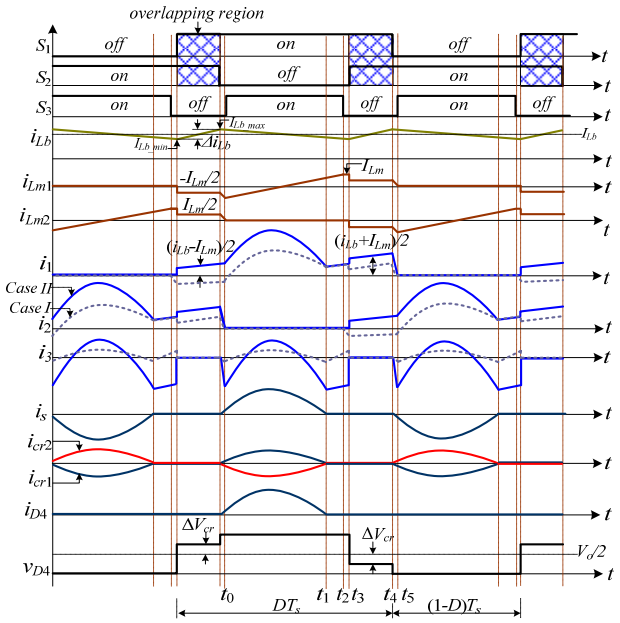

Fig. 2. Key theoretical waveforms of the proposed converter

Interval 1 [See Fig.3(a), $t_0 \leqslant t < t_1$]: At t_0, S_3 is turned on with ZVS. In this interval, the auxiliary switch S_3 and switch S_1 are on, switch S_2 is off and the secondary diode D_4 is forward-biased for freewheeling. Power is transferred from input to output. During this interval, the clamping voltage V_c effects on the primary winding N_{p1} causing nV_c across the secondary winding N_s. Then the leakage inductor L_{lk} resonates with C_{r1} and C_{r2} due to the voltage difference between nV_c and v_{cr1}.The state equation of this stage can be written as

$$L_{lk}\frac{di_s(t)}{dt} = nV_c - v_{cr1}(t) \tag{1}$$

$$i_s(t) = C_{r2}\frac{dv_{cr2}(t)}{dt} - C_{r1}\frac{dv_{cr1}(t)}{dt} \tag{2}$$

$$V_o = v_{cr1}(t) + v_{cr2}(t) \tag{3}$$

where v_{cr1} and v_{cr2} are the voltages across C_{r1} and C_{r2}, respectively. Solving (1)~(3), the secondary current i_s and the voltage across C_{r1} can be calculated as

$$\begin{aligned} i_s(t) &= [(nV_c - v_{cr1}(t_0))/Z_r]\sin\omega_r(t-t_0) \\ &= I_{speak}\sin\omega_r(t-t_0) \end{aligned} \tag{4}$$

$$v_{cr1}(t) = nV_c - [nV_c - v_{cr1}(t_0)]\cos\omega_r(t-t_0) \tag{5}$$

where I_{speak} is the peak value of i_s. The resonant impedance Z_r and the angular resonant frequency ω_r are given by

$$Z_r = \sqrt{L_{lk}/2C_r} \tag{6}$$

$$\omega_r = 1/\sqrt{2L_{lk}C_r} \tag{7}$$

Since the capacitance of C_{r1} is equal to that of C_{r2} and the voltage-doubler rectifier is the same as that of a half-bridge circuit, the discharging current of C_{r2} and the charging current of C_{r1} pass through D_4 together and they can be given by

$$i_{cr1}(t) = -i_{cr2}(t) = i_s(t)/2 \tag{8}$$

The transformer magnetizing current i_{Lm} and the switch currents i_1 and i_3 during this interval can be derived as

$$i_{Lm}(t) = i_{Lm1}(t) = i_{Lm1}(t_0) + V_c(t-t_0)/L_m \tag{9}$$

$$i_1(t) = ni_s(t) + i_{Lm1}(t) \tag{10}$$

$$i_3(t) = i_1(t) - i_{Lb}(t) \tag{11}$$

where the input inductor current decreases linearly resulting from the voltage difference between V_{in} and V_c. It can be calculated by

$$i_{Lb}(t) = I_{Lb\_\max} + (V_{in} - V_c)(t-t_0)/L_b \tag{12}$$

where I_{Lb_max} is the peak value of i_{Lb}.

When the secondary current i_s resonates to zero at t=t_1, this stage is over. Switch current i_1 reaches the magnetizing current i_{Lm1} and i_3 reaches the input inductor current i_{Lb}.

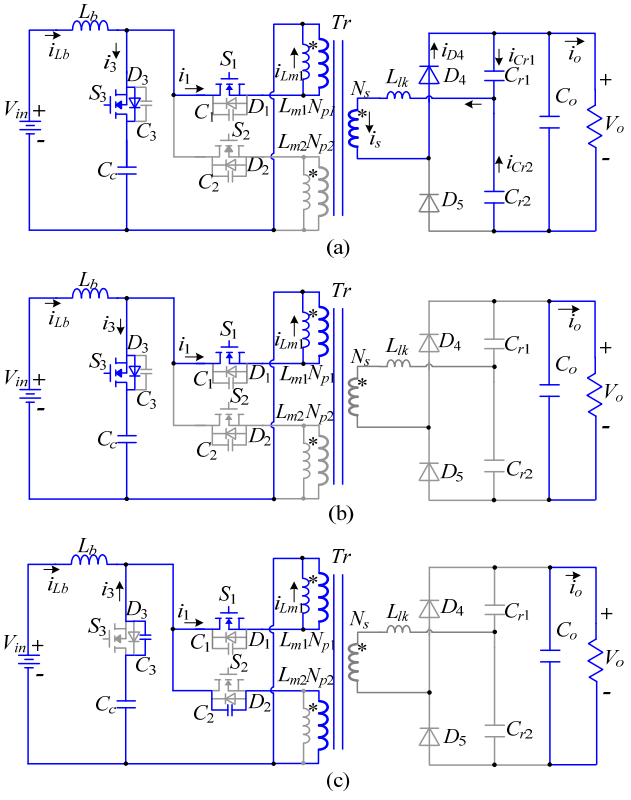

This article has been accepted for publication in a future issue of this journal, but has not been fully edited. Content may change prior to final publication. Citation information: DOI 10.1109/TIE.2016.2638800, IEEE Transactions on Industrial Electronics

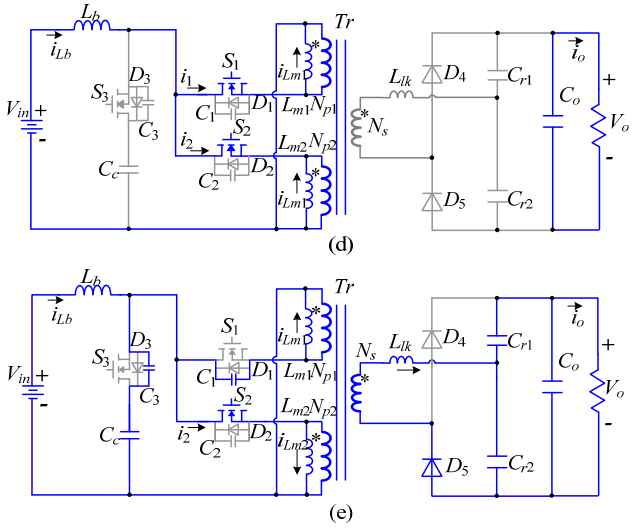

Fig. 3. The corresponding equivalent circuits for each interval (a)~(e): Interval 1~ Interval 5

Interval 2 [See Fig.3(b), $t_1 \leqslant t<t_2$]: At $t=t_1$, the secondary current i_s decreases to zero and the diode D_5 is switched off with zero current, which eliminates the reverse recovery problem. The input current i_{Lb} decreases with the same slope as interval 1. During this interval, the magnetizing current flows through the switch S_1. The primary currents i_1 and i_3 can be expressed by

$$i_1(t) = i_{Lm1}(t) = i_{Lm1}(t_1) + V_c(t-t_1)/L_m \quad (13)$$

$$i_3(t) = i_{Lm1}(t) - i_{Lb}(t) \quad (14)$$

This interval is end when the switch S_3 is turned off at $t=t_2$, and at that time, currents i_{Lb} and i_{Lm1} reach their minimum and maximum values I_{Lb_min} and I_{Lm}, respectively.

Interval 3 [$t_2 \leqslant t<t_3$]: At t_2, S_3 is turned off. The direction of current i_3 at t_2 determines whether the voltage across C_3 will be charged to V_c, which further determines the following two cases. Both of them are described as follows:

Case I) [See Fig.3(c)]: Switch current i_3 is positive at $t=t_2$, as shown in Fig.3(c), that implies $I_{Lm}>I_{Lb\_min}$,. When S_3 is turned off, the current difference between I_{Lm} and I_{Lb_min} charges C_3 and discharges C_2, the voltages across the capacitor C_2 and C_3 can be expressed by

$$v_{C2}(t) = V_c - (I_{Lm} - I_{Lb\_\min})(t-t_2)/(2C) \quad (15)$$

$$v_{C3}(t) = (I_{Lm} - I_{Lb\_\min})(t-t_2)/(2C) \quad (16)$$

At t_3, the voltage v_{C3} increases to V_c and v_{C2} decays to zero, then, D_2 conducts providing ZVS condition for S_2.

Case II): Switch current i_3 is negative, that also means $I_{Lm}<I_{Lb\_min}$. In that case, the input current flows through the antiparallel body diode D_3 until the next interval coming. The equivalent circuit is same with Fig.3 (b).

In fact, *Case I)* only appears when the load varies light. Main switches S_1 and S_2 can achieve ZVS turn-on in that case, which can reduce the switching loss and improve the efficiency.

Interval 4 [See Fig.3(d), $t_3 \leqslant t<t_4$]: At $t=t_4$, the switch S_2 is turned on with ZVS under the condition of *Case I),* while S_2 is hard-switching on and the current that had been passing through D_3 flows into S_2. The voltage across all the windings of Tr is zero since main switches S_1 and S_2 are on and the input current i_{Lb} increases linearly as

$$i_{Lb}(t) = I_{Lb\_\min} + V_{in}(t-t_3)/L_b \quad (17)$$

In this interval, due to the transformer flux balance relation and zero windings voltage, the magnetizing current is provided by two windings commonly. i_{Lm1} decreases from I_{Lm} to $I_{Lm}/2$ and i_{Lm2} increases from zero to $-I_{Lm}/2$ reversely. The input inductor current i_{Lb} is equally divided and flows into S_1 and S_2 and therefore, switch currents i_1 and i_2 can be obtained as

$$i_1(t) = [i_{Lb}(t) + I_{Lm}]/2 \quad (18)$$

$$i_2(t) = [i_{Lb}(t) - I_{Lm}]/2 \quad (19)$$

Moreover, the secondary rectifier diodes D_4 and D_5 are reverse biased and the output capacitor C_o offers energy to the load during this interval. The voltage across the secondary diode D_4 can be given by

$$v_{D4} = V_o/2 - \Delta V_{cr} \quad (20)$$

where ΔV_{cr} is the maximum capacitor voltage ripple, as shown in Fig.2, which can be deviation from the average voltage.

$$\Delta V_{cr} = I_o T_s/[2(C_{r1}+C_{r2})] \quad (21)$$

Interval 5 [See Fig.3(e), $t_4 \leqslant t<t_5$]: At $t=t_5$, the input current reaches its maximum value I_{Lb_max} and main switch S_1 is turned off. In this short time, the current through S_1 is diverted into the auxiliary switch path causing the capacitor C_1 charges to $2V_c$ and C_3 discharges to zero quickly. Then, D_3 conducts providing ZVS turn-on condition for S_3.

In this interval, the magnetizing current that had been flowing through the wingding N_{p1} transfers to N_{p2} and secondary current i_s starts slowly rising reversely due to the decrease of primary current i_1.

After $t=t_5$, S_3 is turned on with ZVS and the latter half-cycle interval begins working, and the operation principle is similar with that of the former half-cycle and not be clarified again.

III. Analysis and Design of the Converter

A. Output Characteristics

From (5), it can be gotten that the average voltage value of v_{cr1} is nV_c., and the v_{cr2} has the same average value. Moreover, since the sum of v_{cr1} and v_{cr2} is V_o, the relation between V_o and V_c can be expressed as

$$V_o = 2nV_c \quad (22)$$

According to the volt-second balance principle of inductor L_b during the half switching period, the relation between the voltage V_{in} and V_c can be given by

$$V_{in}(D-0.5) + (V_{in}-V_c)(1-D) = 0 \quad (23)$$

Solving (23), the voltage V_c can be obtained as

$$V_c = V_{in}/[2(1-D)] \quad (24)$$

Therefore, the voltage gain can be derived as follows:

$$V_o = nV_{in}/(1-D) \quad (25)$$

From (25), it can be seen that the voltage gain becomes that of an isolated boost converter. It means that the proposed converter performs step-up function to interface the fuel cell for conditioning power.

This article has been accepted for publication in a future issue of this journal, but has not been fully edited. Content may change prior to final publication. Citation information: DOI 10.1109/TIE.2016.2638800, IEEE Transactions on Industrial Electronics

B. Input Current Ripple

From the steady-state operation, the input current i_{Lb} increases with a slope of V_{in}/L_b and the duration time is $(D\text{-}0.5)T_s$. Thus, the ripple current of L_b can be calculated by

$$\Delta I_{Lb} = \frac{V_{in}}{L_b}(D-0.5)T_s \tag{26}$$

Substituting (25) into (26), it can be expressed as

$$\Delta I_{Lb} = \frac{V_o(1-D)(D-0.5)}{nL_b f_s} \tag{27}$$

where f_s is the switching frequency.

C. Soft-Switching Characteristics and the Selection of C_{r1} and C_{r2}

According to the analysis of Interval 3 in section-II, main switches S_1 and S_2 achieve ZVS turn-on with the condition of $I_{Lm}>I_{Lb\_min}$. which can be further derived approximately as

$$I_o < \frac{V_o(1-D)\eta}{4n^2 L_m f_s} \tag{28}$$

where η represents the conversion efficiency.

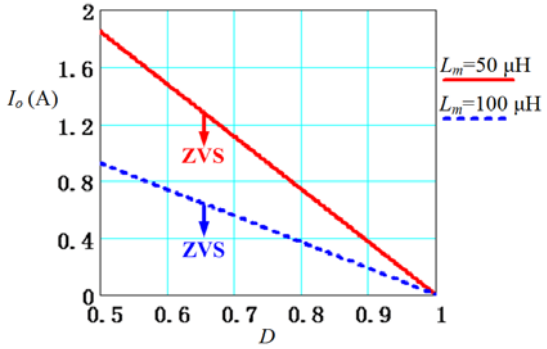

Fig. 4. The ZVS load range for main switches S_1 and S_2 for the given specification of V_o=350 V, n=3, η=0.95 and f_s=50KHz

Fig.4 shows the ZVS load range (the relation between load current I_o, duty cycle D and magnetizing inductance L_m) of switches S_1 and S_2 for the given specifications of the output voltage V_o=350 V, turns ratio n=3, switching frequency f_s=50 KHz and conversion efficiency η=0.95. Note here that S_1 and S_2 can achieve ZVS turn-on if the converter works under the curve region. It can be seen that the ZVS load range varies wide with the decrease of duty cycle D and magnetizing inductance L_m. However, it is noted that the smaller magnetizing inductance L_m results in higher conduction loss. So it should make a tradeoff between them in design of L_m.

The ZVS turn-on of primary switches S_3 can be achieved since the current had been passing through S_1 (S_2) forces to flows through D_3 when S_1 (S_2) is turned off. The energy stored in the input inductor is relatively large at rated or light load in low voltage, high current applications. So the ZVS of S_3 can be achieved easily, which can reduce the switching loss.

To minimize the switching losses of the diodes D_4 and D_5, secondary current i_{D4} (i_{D5}) has to resonant to zero before t_3. From (4), to ensure diodes D_4 and D_5 realize ZCS, secondary current i_s needs to satisfy

$$i_s(t_1) = I_{speak}\sin\omega_r[(1-D_{\max})T_s] = 0 \tag{29}$$

where D_{max} is the maximum duty ratio.

From (29), the resonant switching f_r can be derived as

$$f_r = \frac{f_s}{2(1-D_{\max})} \tag{30}$$

Therefore, for ZCS of secondary diodes D_4 and D_5, C_{r1} and C_{r2} can be design as

$$C_{r1} = C_{r2} = C_r < \frac{(1-D_{\max})^2}{(\pi f_s)^2 L_{lk}} \tag{31}$$

D. Voltage Stress and RMS Current

According to the foresaid operational intervals, the voltage stress of switches S_1~S_3 and rectifier diodes D_4~D_5 can be expressed as

$$V_{s1} = V_{s2} = 2V_c = V_{in}/(1-D) \tag{32}$$

$$V_{s3} = V_c = V_{in}/[2(1-D)] \tag{33}$$

$$V_{D4} = V_{D5} = V_o \tag{34}$$

The rms current of main switches S_1 and S_2 can be calculated as (35) and that of the auxiliary switches S_3 can be acquired as (36). The diode rms current can be calculated from

$$I_{diode(rms)} = \sqrt{\frac{1}{T_s}\int_0^{\pi\sqrt{2L_{lk}C_r}} \left(\frac{nV_c - V_{cr}}{Z_r}\sin\omega_r t\right)^2 dt} \tag{37}$$

IV. Topologies Comparison

In this section, the conventional push-pull converter with center-tap rectifier, ZVS clamping mode current-fed push-pull converter [37] and the current-fed push-pull resonant converter [40] are selected for performance comparison due to the similarity in circuit structure, characteristics and the suitable fuel cell application. Table I summarizes the findings from this investigation.

The comparison in Table I provides detailed characteristics for all four topologies. It is clear that each topology has its advantages and disadvantages. Overall, since soft-switching, lower voltage stress, and low flux imbalance risk can be realized with the proposed converter, the proposed converter is a good candidate for the fuel cell application. Noticeably, the proposed converter with fewer components but has similar characteristics with the previous current-fed push-pull converters. This aspect makes it lower cost and higher reliability. Moreover, due to soft-switching at light load condition, this converter may maintain higher efficiency than its similar converter that is hard-switched [3],[39]-[40].

$$I_{S_1\&S_2(rms)} = \sqrt{\frac{1}{T_s}\int_0^{\pi\sqrt{2L_{lk}C_r}} \left[n\left(\frac{nV_c - V_{cr}}{Z_r}\sin\omega_r t\right) + \left(\frac{V_c}{L_m}t - I_{Lm}\right)\right]^2 dt + \frac{1}{T_s}\int_0^{(D-0.5)T_s} \frac{I_{Lm}^2 + I_{Lb}^2}{2} dt + \frac{1}{T_s}\int_0^{((1-D)T_s - \pi\sqrt{2L_{lk}C_r}} \left[i_{Lm}(t_1) + \frac{V_c}{L_m}(t-t_1)\right]^2 dt} \tag{35}$$

$$I_{S_3(rms)} = \sqrt{\frac{2}{T_s}\int_0^{\pi\sqrt{2L_{lk}C_r}} \left[n\left(\frac{nV_c - V_{cr}}{Z_r}\sin\omega_r t\right) + \left(\frac{V_c}{L_m}t - I_{Lm}\right) - I_{Lb}\right]^2 dt + \frac{2}{T_s}\int_0^{(1-D)T_s - \pi\sqrt{2L_{lk}C_r}} \left[i_{Lm}(t_1) + \frac{V_c}{L_m}(t-t_1) - I_{Lb}\right]^2 dt} \tag{36}$$

This article has been accepted for publication in a future issue of this journal, but has not been fully edited. Content may change prior to final publication. Citation information: DOI 10.1109/TIE.2016.2638800, IEEE Transactions on Industrial Electronics

TABLE I
COMPARISON OF FOUR TOPOLOGIES

		Conventional push-pull converter	ZVS clamping mode current-fed Push-Pull converter in[37]	Current-fed push-pull resonate converter in [40]	The proposed current-fed push-pull converter
Total components	**Primary side devices**	2 MOSFETs + 1 Inductor	4 MOSFETs + 1 Capacitor+1 Inductor	4 MOSFETs +1 Inductor +2 Capacitors	3 MOSFETs +1 Inductor+1 Capacitor
	Secondary side devices	2 Diodes+2 Inductors+1 Filter capacitor	2 Diodes+1 Filter capacitor	2 Diodes +2 Resonant capacitors+1 Filter capacitor	2 Diodes +2 Resonant capacitors +1 Filter capacitor
Voltage stress	**Primary side switches**	$>2V_{in}$	$2V_{in}/(1\text{-}D)$	$V_{in}/(1\text{-}D)$	Main switches: $V_{in}/(1\text{-}D)$ Auxiliary switch: $V_{in}/2(1\text{-}D)$
	Secondary side diodes	$2V_o$	V_o	V_o	V_o
Switching features	**Primary side switches**	Harding switching	ZVS	Harding switching	ZVS at light load
	Secondary side diodes	Harding switching	Hard switching	ZCS	ZCS
Switching losses		High	Relative low	Relative low	Low
Leakage inductor energy recovery		No	Yes	Yes	Yes
Conversion voltage gain		$2nDV_{in}$	$nV_{in}/(1\text{-}D)$	$2nV_{in}/(1\text{-}D)$	$nV_{in}/(1\text{-}D)$
Flux imbalance risk		High	Low	Low	Low
Driver Circuit		Simplicity (non-isolation)	Difficulty (half-isolation)	Difficulty (half-isolation)	Difficulty (isolation)

V. EXPERIMENTAL RESULTS

In order to verify the effectiveness of the proposed converter, a 510 W experimental prototype controlled by a DSP28335 digital signal processor was built, the experimental results along with loss breakdown are presented in this section. The specifications are listed in Table II. Fig. 5 shows the photograph of implemented prototype.

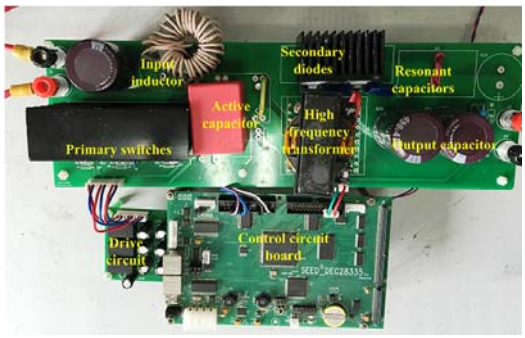

Fig. 5 The photograph of implemented prototype.

TABLE II
COMPONENTS AND KEY PARAMETERS OF THE PROTOTYPE

Components	Parameters
Input voltage	30~50V DC
Output voltage	350 V DC
Switching frequency (S_3)	100 KHz
Output rated power	510 W
Primary switches: S_1~S_3	FDPF190N15A/V_{DSS}=150V, I_D=27.4, R_{dson}=19mΩ.
Transformer turns ratio	ETD49/N87 (turns ratio: N_{P1}:N_{P2}:N_s =4:4:12) Leakage inductance L_{lk}=2.5 μH, Magnetizing inductance L_{m1}= L_{m2}=50 μH.
Input inductance	MPP 55076A2 /L_b=45 μH
Secondary diodes: D_4~D_5	SF5A400H/V_{RRM}=400V, $I_{F(AV)}$=5 A
Resonant capacitor C_{r1}, C_{r2}	0.47μF
Clamping capacitor C_c	10 μF /200V film capacitor
Output filter capacitors C_o	470 μF

From (32) and (33), the voltage V_c determines the voltage stress across the primary switches and it should be designed rather low enabling the use of low $R_{ds(on)}$ devices. Here, the voltage V_c can be selected as near 60V that is lower than 1.2 times of the maximum V_{in}. The range of duty cycle at the specified input voltage can be calculated as 0.57~0.74. The leakage inductance of HF transformer L_{lk} is measured about 2.5 μH and the magnetizing inductance L_m is obtained as 50 μH. This implies switches S_1&S_2 can achieve ZVS turn-on under near 1A load current at the maximum duty cycle 0.74, which can be seen from Fig. 4. In addition, by (30) and (31), the resonant frequency f_r can be designed as 100 KHz to ensure ZCS of the secondary diodes and the resonate capacitors are opted as 0.47 μF. The input inductance L_b can be designed as 45 μH that causes about 20% maximum rated current ripple at the maximum duty cycle.

The experimental results of the prototype under different output power and input voltage conditions are shown in Fig.6 and Fig.7, respectively. Fig.6 shows the tested waveforms for V_{in}=30 V at the rated load (510 W) and Fig.7 shows that for V_{in}=50V at near 20% rated load (100W). It can be seen that the results match closely with analytically steady-state operation in section II.

Parts (a) of Fig.6 and Fig.7 show the gate signal v_{gs3}, switch voltage v_{ds3} and switch current i_3 waveforms of the auxiliary switch S_3. Obviously, the body diode of S_3 conducts prior to switch conduction that confirming ZVS turn-on is achieved for S_3, either under the rated load or the light load. The steady-state voltage across S_3 equals to near 60 V, which matches with the above designed value.

Parts (b) of Fig.6 and Fig.7 present the gate signal v_{gs1}, switch voltage v_{ds1} and switch current i_1 waveforms of the main switch S_1. It can be seen that the ZVS performance of S_1 is lost with the converter operates at rated load. However, it can realize ZVS

This article has been accepted for publication in a future issue of this journal, but has not been fully edited. Content may change prior to final publication. Citation information: DOI 10.1109/TIE.2016.2638800, IEEE Transactions on Industrial Electronics

turn-on at a rather light load by utilization of the magnetizing current that enabling to reduce the switching loss and improve the efficiency. Also, it can be observed that the voltage across switch S_1 is about two times of V_c that is less than 120 V. The other main switch S_2 has the same waveforms due to the symmetrical operation.

Parts (c) of Fig.6 and Fig.7 illustrate the current and voltage waveforms of the secondary diode D_4. Diode current i_{D4} reaches zero before D_4 is reversely biased either under rated load or under light load that ensures ZCS of the diode. Therefore, the reverse-recovery problem of diodes D_4 and D_5 can be released and their switching losses are reduced. Moreover, it can be obtained that the secondary resonant frequency is near 100 KHz, which is about the same as the designed value.

Parts (d) of Fig.6 and Fig.7 show the waveforms of gate signal v_{gs3}, the input current i_{Lb} and the secondary current i_s. It can be observed that the maximum current ripple occurs at the minimum input voltage, which agrees with the aforesaid in the Section-II.

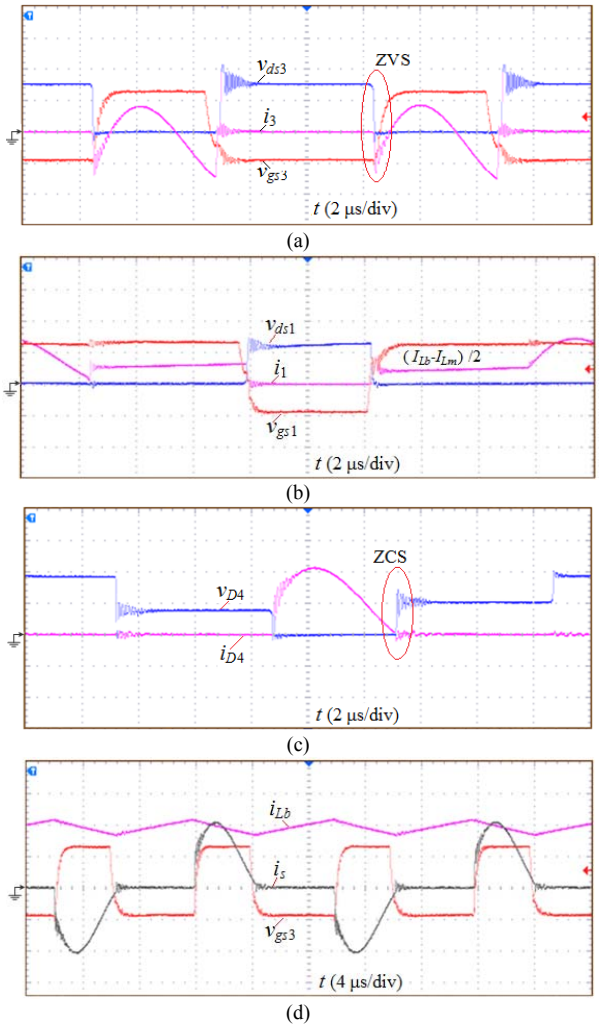

Fig. 6 Experimental waveforms at V_{in}=30V and rated power. (a) Auxiliary switch S_3 voltages v_{gs3} (10 V/div), v_{ds3} (4 V/div) and switch current i_3 (10 A/div). (b) Main switch S_1 voltages v_{gs1} (10 V/div), v_{ds1} (100 V/div) and switch current i_1 (20 A/div). (c) Secondary diode D_4 voltage v_{D4} (200 V/div) and current i_{D4} (5 A/div). (d) Switch S_1 voltages v_{gs3} (20 V/div), input inductance current i_{Lb} (10 A/div) and secondary current i_s (5 A/div)

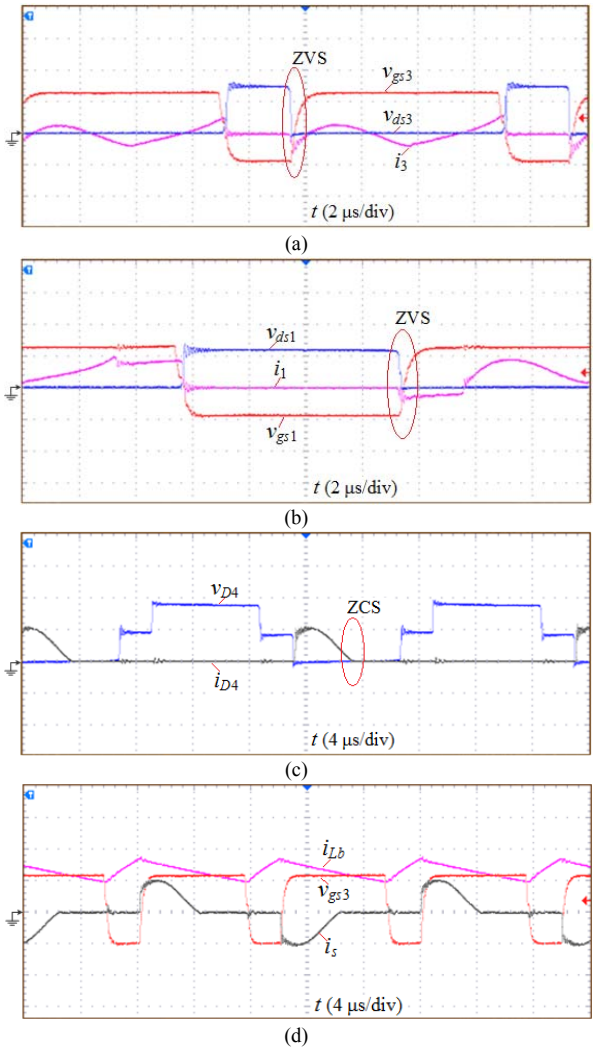

Fig. 7 Experimental waveforms at V_{in}=50V and 20% rated power. (a) Auxiliary switch S_3 voltages v_{gs3} (10 V/div), v_{ds3} (40 V/div) and switch current i_3 (5 A/div). (b) Main switch S_1 voltages v_{gs1} (10 V/div), v_{ds1} (100 V/div) and switch current i_1 (5 A/div). (c) Secondary diode D_4 voltage v_{D4} (200 V/div) and current i_{D4} (2 A/div). (d) Switch S_1 voltages v_{gs3} (10 V/div), input inductance current i_{Lb} (2 A/div) and secondary current i_s (2 A/div)

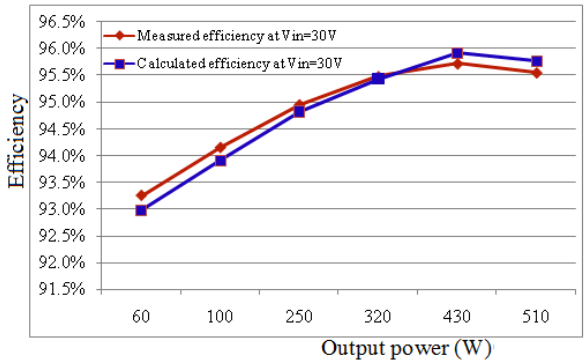

(a)

This article has been accepted for publication in a future issue of this journal, but has not been fully edited. Content may change prior to final publication. Citation information: DOI 10.1109/TIE.2016.2638800, IEEE Transactions on Industrial Electronics

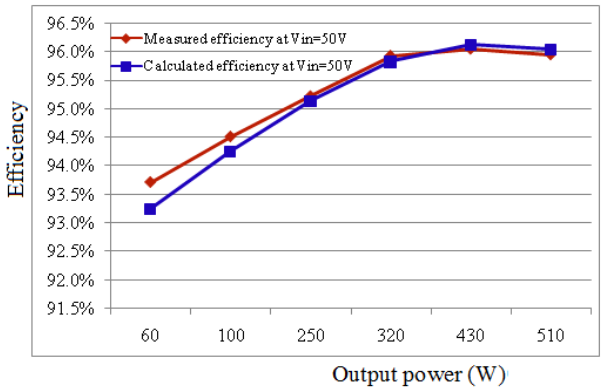

(b)

Fig. 8 The measured and calculated efficiency curves of the prototype with V_{in}=30V and V_{in}=50V.

From parts (a)~(c) of Fig.6 and Fig.7, the voltage spikes across all switches and diodes are suppressed. However, due to stray inductances owing to wiring connections, device capacitances and parasitics in the PCB board, some ringing can be also observed during the switching transient. Moreover, the ringing increases with increase in output power since the larger current through them results in larger oscillation energy. These oscillations can be also noticed in the reported active-clamped current-fed converters [3], [12] and [41], and they have the similar cause of ringing.

TABLEIII
LOSS DISTRIBUTION ASSESSMENT OF THE PROPOSED CONVERTER UNDER DIFFERENT OUTPUT POWER

		V_{in}=50V,P_o=60 W Power loss (W)	V_{in}=30V,P_o=510W Power loss (W)
Switches S_1~S_3 switching loss	Turn-on loss	0	2.625
	Turn-off loss	0.399	4.909
Switch S_1~S_3 conduction loss		0.268	4.765
Gate driver loss		0.090	0.090
Diodes D_4~D_5 conduction loss		0.240	2.040
Input inductor loss	Core loss	0.181	1.150
	Conduction loss	0.014	2.890
High frequency transformer loss	Core loss	3.157	1.716
	Conduction loss	0.070	2.345
Calculated total loss		4.419	22.53
Calculated efficiency		93.141%	95.769%

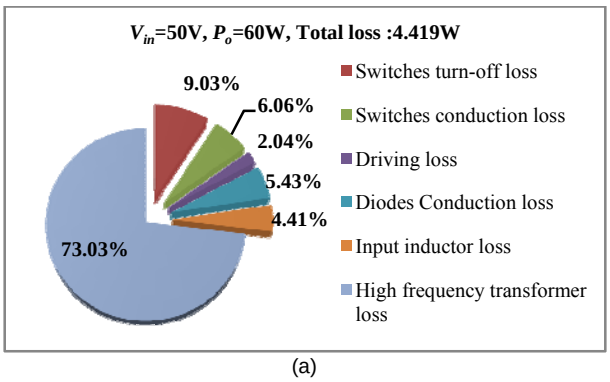

(a)

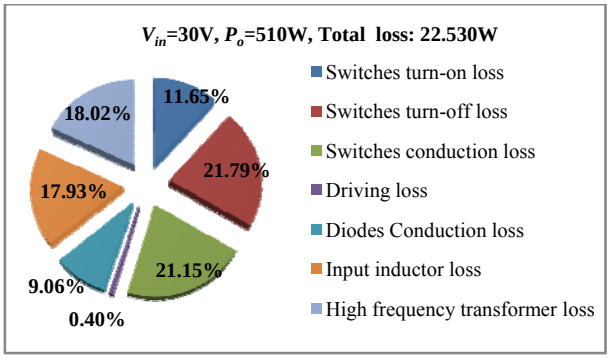

(b)

Fig.9 Loss breakdown of the prototype at different output power with V_{in}=50 V and V_{in}=30 V.

Fig. 8(a) and (b) show the measured and calculated efficiency curves of the prototype with different output power at V_{in}=30V and V_{in}=50V, respectively. The measured efficiency can reach or exceed 96.12% for V_{in}=50V and 95.72% for V_{in}=30V. It can be observed from these curves that the tested values coincide with the calculated values approximately. Here, the loss calculated models given in [44] and [45] are used to assess the power loss and the loss distribution of the prototype at different output power. Table III and Fig.9 show the loss distribution assessment at the 60 W load with V_{in}=50 V and the rated load with V_{in}=30 V. It is easy to find that the conduction loss in the low load is small because of the utilization of low-voltage devices. A considerable part of loss is the core loss of the transformer, which is the dominant loss in the 60W load since the low duty cycle produces a rather peak flux density resulting in rather higher core loss. However, this portion loss can be reduced with the rising of power level and optimized design.

VI. CONCLUSION

A simple high step-up current-fed push-pull quasi-resonant converter for fuel cell power system was presented in this paper. By employing the current-fed structure and voltage-doubler rectifier, a much higher voltage conversion ratio was achieved without large turns-ratio of transformer. ZVS can be realized for all of three primary switches at light load and ZCS can be achieved for the secondary diodes in the full load range by the resonant condition. The voltage-doubler rectifier eliminates the reverse-recovery problem of rectifier diodes and the auxiliary active-clamp circuit suppresses the voltage spike of switches and recycled the energy stored in the leakage inductance. Moreover, compared with the reported topologies, this converter realizes the similar features with fewer components, which reduces the cost and improves system reliability. A 510W prototype was implemented to verify the analysis and performance. The prototype achieved a high efficiency of 96.12% at an input voltage of 50 V.

REFERENCES

[1] Global Renewable Energy Status and Medium-term Outlook until 2018. [online].Available: :https://cleanenergysolutions.org/training/global-renewable-energy-status-and-medium-term-outlook-until-2018

[2] A. Pilloni, A. Pisano, E.Usai, "Observer-based air excess ratio control of a PEM fuel cell system via high-order sliding mode", *IEEE Trans. Ind. Electron.*, vol. 62, no. 8, pp. 5236 - 5246, Aug. 2015.

[3] V. Vaisanen, T. Riipinen, J. Hiltunen, and P. Silventoinen, "Design of 10 kW resonant push-pull DC-DC converter for solid oxide fuel cell applications," in *Proc. IEEE EPE*, 2011, pp. 1-10.

[4] J. Wang, F. Z. Peng, J. Anderson, A. Joseph, and R. Buffenbarger, "Low cost fuel cell converter system for residential power generation," *IEEE Trans. Power Electron.*, vol. 19, no. 5, pp. 1315–1322, Sep. 2004.

[5] M. Nymand and M. A. E. Andersen, "High-efficiency isolated boost dc–dc converter for high-power low-voltage fuel-cell applications," *IEEE Trans. Ind. Electron.*, vol. 57, no. 2, pp. 505–514, Feb. 2010

[6] A. Averberg and A. Mertens, "Analysis of a voltage-fed full bridge dc–dc converter in fuel cell systems," in *Proc. 38th IEEE PESC*, Miami, FL, 2007, pp. 286–292.

[7] Z. Zhang, O. C. Thomsen, and M. A. E. Andersen, "Soft-switched dual-input DC–DC converter combining a boost-half-bridge cell and a voltage-fed full-bridge cell," *IEEE Trans. Power Electron.,* vol. 28, no. 11, pp. 4897–4902, Nov. 2013.

[8] Y. Yuan and Q. Wu, "One zero-voltage-switching three-transistor push–pull converter," *IET Power Electron.*, vol. 6, no. 7, 2013, pp. 1270–1278..

[9] R. Gopinath, S. Kim, Ja.-H. Hahn, P. N. Enjeti, M. B. Yeary, and J. W. Howze, "Development of a low cost fuel cell inverter system with dsp control," *IEEE Trans. Power Electron.*, vol. 19, no. 5, pp. 1256–1262, Sep. 2004.

[10] C. Ekkaravarodome and K. Jirasereeamornkul, "Analysis and implementation of a half bridge class-de rectifier for front-end ZVS push-pull resonant converters," *Journal of Power Electron*., Vol. 13, No. 4, pp. 626-635, July 2013.

[11] A. Averberg, K. R. Meyer, and A. Mertens, "Current-fed full bridge converter for fuel cell systems," in *Proc. IEEE Power Electron. Spec. Conf.*, 2008, pp. 866–872.

[12] U. R. Prasanna and A. K. Rathore, "Extended range ZVS active-clamped current-fed full-bridge isolated dc/dc converter for fuel cell applications: Analysis, design and experimental results," *IEEE Trans. Ind. Electron.*, vol. 60, no. 7, pp. 2661–2672, Jul. 2013.

[13] X. Kong and A. M. Khambadkone, "Analysis and implementation of a high efficiency, interleaved current-fed full bridge converter for fuel cell system," *IEEE Trans. Power Electron.*, vol. 22, no. 2, pp. 543–550, Mar.2007.

[14] H. Kim, C. Yoon, and S. Choi, "An improved current-fed ZVS isolated boost converter for fuel cell application," *IEEE Trans. Power Electron.*,vol. 25, no. 9, pp. 2357–2364, Sep. 2010

[15] M. Mohr and F.-W. Fuchs, "Voltage fed and current fed full bridge converter for the use in three phase grid connected fuel cell systems," in *Proc. IEEE Int.* Power *Electron. Motion Control Conf.*, 2006, pp. 1–7.

[16] A. K. Rathore and U. Prasanna, "Comparison of soft-switching voltage-fed and current-fed bi-directional isolated DC/DC converters for fuel cell vehicles," in *Proc. IEEE Int. Symp. Ind. Electron.*, May 2012, pp. 252–257.

[17] K. Radhasree and A. K. Rathore, "Hybrid modulated extended secondary universal current-fed ZVS converter for wide voltage range: Analysis, design, and experimental results," *IEEE Trans. Ind. Electron.*, vol. 62, no. 7, pp. 4471–4480, Jul. 2015.

[18] A. K. Rathore, A. K. S. Bhat, and R. Oruganti, "Analysis, design, and experimental results of wide range ZVS active-clamped L-L type current-fed dc/dc converter for fuel cells to utility interface," *IEEE Trans. Ind. Electron.*, vol. 59, no. 1, pp. 473–485, 2012.

[19] S. J. Jang, C. Y. Won, B. K. Lee, and J. Hur, "Fuel cell generation system with a new active clamping current-fed half-bridge converter," *IEEE Trans. Energy* Convers., vol. 22, no. 2, pp. 332–340, Jun. 2007.

[20] Y. Zhao, W. Li, Y. Deng, X. He, "Analysis, Design, and Experimentation of an Isolated ZVT Boost Converter With Coupled Inductors," *IEEE Trans. Power Electron.*, vol. 26, no. 2, pp. 466–475, Feb. 2011.

[21] W. Li, D. Xu, B. Wu, Y. Zhao, H. Yang, X. He, "Zero-voltage-switching dual-boost converter with multi-functional inductors and improved symmetrical rectifier for distributed generation systems," *IET Power Electron.*, vol. 5, no. 7, pp. 969–977, 2012.

[22] J. M. Kwon and B. H. Kwon, "High step-up active-clamp converter with input-current doubler and output-voltage doubler for fuel cell power systems," *IEEE Trans. Power Electron.*, vol. 24, no. 1, pp. 108–115, Jan. 2009.

[23] P. M. Barbosa and I. Barbi, "A single-switch flyback-current-fed dc–dc converter," *IEEE Trans. Power Electron.*, vol. 13, no. 3, pp. 466–475, May. 1998.

[24] N. T. Quang, H. Chiu, Y. Lo, M. M. Alam, "Zero-voltage switching current-fed flyback converter for power factor correction application," *IET Power Electron.*, vol. 6, no. 9, pp. 1971–1978, 2013.

[25] W. Li, L. Fan, Y. Zhao, X. He, D. Xu, and B. Wu, "High-step-up and high-efficiency fuel-cell power-generation system with active-clamp flyback–forward converter," *IEEE Trans. Ind. Electron.*, vol. 59, no. 1, pp. 599–610, Jan.2012.

[26] W. Li; Y. Zhao; X. He; D. Xu; B. Wu, "Interleaved ZVS flyback-forward converter with reduced output voltage stress on secondary rectifier diodes," in *Proc. IEEE Appl. Power Electron. Conf.*, 2011, pp. 1915–1919.

[27] S. Ohtsu, T. Yamashita, K. Yamamoto, and T. Sugiura, "Stability in high-output-voltage push-pull current-fed converters," *IEEE Trans. Power Electron.*, vol. 8, no. 2, pp. 135–139, Apr. 1993.

[28] A. L. Rabello, M. A. Co, D. S. L. Simonetti, and J. L. F. Vieira, "An isolated DC–DC boost converter using two cascade control loops," in *Proc. IEEE ISIE*, Jul. 1997, vol. 2, pp. 452–456.

[29] A. H. Weinberg and L. Ghislanzoni, "A new zero voltage and zero current power switching technique," *IEEE Trans. Power Electron.*, vol. 7, no. 4, pp. 655–665, Oct. 1992.

[30] C. L. Chu and C. H. Li, "Analysis and design of a current-fed zero-voltage switching and zero-current-switching CL-resonant push-pull DC–DC converter," *IET Power Electron.*, vol. 2, no. 4, pp. 456–465, Jul. 2009.

[31] Y. H. Kim, S. C. Shin, J. H. Lee, Y. C. Jung, and C. Y. Won, "Soft switching current-fed push-pull converter for 250-W AC module applications," *IEEE Trans. Power Electron.*, vol. 29, no. 2, pp. 863–872, Feb.2014.

[32] D. J. Thrimawithana, and U. K. Madawala, "Analysis of split-capacitor push–pull parallel-resonant converter in boost mode," *IEEE Trans. Power* Electron., vol. 23, no. 1, pp. 359–368, Feb.2008.

[33] K. R. Sree, and A. K. Rathore, "Impulse commutated zero-current switching current-fed push–pull converter: analysis, design, and experimental results," *IEEE Trans. Ind. Electron.*, vol. 62, no. 1, pp. 363–370, Jan. 2015.

[34] I. Barbi and R. Gules, "Isolated DC-DC converters with high-output voltage for TWTA telecommunications satellite applications," *IEEE Trans. Power Electron.*, vol. 18, no. 4, pp. 975–984, Jul. 2003.

[35] J. M. Blanes, A. Garrigos, J. A. Carrasco, J. E. Mart´ı, and E. S. Kilders, "High-efficiency regulation method for a zero-current and zero-voltage current-fed push–pull converter," *IEEE Trans. Power Electron.*, vol. 26, no. 2, pp. 444–452, Feb. 2011.

[36] A.A. Patwardhan, M. S. Deo and M. Mangal, "18 kW DC-DC converter using push-pull inverter with lossless snubber circuits," in *Proc. Power Electron. Drives and Energy Syst. (PEDES)*, Vol.2, pp.789-793, 1996.

[37] F. J. Nome and I. Barbi, "A ZVS clamping mode-current-fed push–pull DC–DC converter," in *Proc. IEEE Int. Symp. Ind. Electron.*, 1998, vol. 2,pp. 617–621.

[38] X. Pan and A. K. Rathore, "Naturally clamped zero-current commutated soft-switching current-fed push–pull DC/DC converter: analysis, design, and experimental results," *IEEE Trans. Power Electron.*, vol. 33,no. 3, pp. 1318–1327, Mar. 2015

[39] E.-H. Kim and B.-H. Kwon, "High step-up resonant push-pull converter with high-efficiency," *IET Power Electron.*, vol. 2, no. 1, pp. 79–89, Jan. 2009.

[40] J.-M. Kwon, E-H. Kim, B.-H. Kwon, and K.-H. Nam, "High-efficiency fuel cell power conditioning system with input current ripple reduction," *IEEE* Trans*. Ind. Electron.*, vol. 56, no. 3, pp. 826–834, Mar. 2009.

[41] S. Lee, J. Park, and S. Choi, "A three-phase current-fed push–pull DC–DC converter with active clamp for fuel cell applications," *IEEE Trans. Power Electron.*, vol. 26, no. 8, pp. 2266–2277, Aug. 2011.

[42] T. C. Lim, B. W. Williams, S. J. Finney, H. B. Zhang, and C. Croser, "Energy recovery snubber circuit for a dc-dc push-pull converter," *IET Trans. Power Electron.*, vol. 5, no. 6, pp. 863–872, Jul. 2012.

[43] B. Whitaker, D. Martin, and E. Cilio, "Extending the operational limits of the push-*p*ull converter with SiC devices and an active energy recovery clamp circuit," in *Proc. IEEE Appl. Power Electron. Conf.*, 2015, pp. 2023–2038.

[44] Z.Wang and H. Li, "A soft switching three-phase current-fed bidirectional DC–DC converter with high efficiency over a wide input voltage range," *IEEE Trans. Power Electron.*, vol. 27, no. 2, pp. 669–684, Feb. 2012.

[45] W. G. Hurley and W. H. Wölfle, "Transformers and inductors for power electronics theory, design and applications," John Wiley & Sons Ltd. Publication, 2013.

Qunfang Wu (S'15**)** received the B.S. and M.S. degrees in electrical engineering from East China Jiaotong University, Nanchang, China, in 2011 and 2014, respectively. He is currently pursuing the Ph.D. degree in electrical engineering with the Nanjing University of Aeronautics and Astronautics, Nanjing, China.

His current research interests include soft switching dc/dc converters, dc/ac soft inverters and gate driver technologies.

Qin Wang (M'10) received the B.S., M.S., and Ph.D. degrees in electrical engineering from the Nanjing University of Aeronautics and Astronautics (NUAA), Nanjing, China, in 1987, 1996, and 2011, respectively. In 1996, he joined the Faculty of Electrical Engineering Teaching and Research Division, NUAA, and became an Associate Professor in 2005 at the College of Automation Engineering, NUAA, where he is currently a Professor with the Jiangsu Key Laboratory of New Energy Generation and Power Conversion. He is the author or coauthor of more than 30 technical papers in journals and conferences and also published three books.

His current research interests include multi-input dc/dc converters, soft switching dc/dc converters and renewable energy generation systems.

Jialin Xu received the B.Sc. degree in electrical engineering and automation from Nanjing University of Aeronautics and Astronautics (NUAA), Nanjing, China, in 2015, where she is currently working toward the Master degree in power electronics and power transmission.

Her research interests include DC/DC converters and DC microgrid operations.

Hongxu Li received the B.E. degree in electrical engineering from Chongqing University, Chongqing, China, in 2013.He is currently pursuing the M.S. degree in electrical engineering with the Nanjing University of Aeronautics and Astronautics, Nanjing, China.

His current research interests include power conversion and control of three-phase power rectifiers/inverters.

Lan Xiao (M'06) received the B.S. and Ph.D. degrees in electrical engineering from Nanjing University of Aeronautics and Astronautics (NUAA), Nanjing, China, in 1993 and 1998, respectively. In 1999, she joined the College of Automation Engineering, NUAA, as a Faculty Member, where she is currently a Professor with the Jiangsu Key Laboratory of New Energy Generation and Power Conversion. She is the author or coauthor of more than 50 technical papers in journals and conferences.

Her current research interests include soft-switching dc/dc converters, soft-switching inverters, and renewable energy generation system.